Chemical Science

ROYAL SOCIETY OF CHEMISTRY

EDGE ARTICLE

View Article Online
View Journal | View Issue

Cite this: *Chem. Sci.*, 2025, **16**, 4295

All publication charges for this article have been paid for by the Royal Society of Chemistry

Targeted anchoring of Cu sites in imine-based covalent organic frameworks as catalytic centers for efficient Li–CO_2 batteries†

Haixia Chen, Zhixin Liu, Yunyun Xu, Xingyu Yu, Yinglei Tao, Yue Li, Xianli Huang, Jianping He and Tao Wang *

Received 5th November 2024
Accepted 23rd January 2025

DOI: 10.1039/d4sc07485h

rsc.li/chemical-science

Lithium–carbon dioxide (Li–CO_2) batteries have attracted much attention due to their high theoretical energy density and reversible CO_2 reduction/evolution process. However, the wide bandgap insulating discharge product Li_2CO_3 is difficult to decompose, leading to large polarization or even death of the battery, thus seriously hindering the practical application of Li–CO_2 batteries. The properties of covalent organic framework (COF) materials, which can support the construction of multiphase catalytic systems, have great potential in the fields of CO_2 enrichment and electrocatalytic reduction. In this paper, the excellent redox properties of transition metal were utilized to introduce Cu metal into an imine-based COF to form Cu–O,N sites as the active sites for CO_2 oxidation and reduction. The electrochemical performance of the Cu sites in Li–CO_2 batteries was investigated, and the prepared batteries were able to cycle stably at a current density of 200 mA g^{-1} for more than 1100 h. COF structural sites can be anchored by metal Cu sites to form Cu–O,N active centers for CO_2 oxidation and reduction processes. This study provides a new approach for the development of lithium CO_2 batteries towards more stable and stable.

Introduction

In order to reduce carbon dioxide (CO_2) emissions and pursue a low-carbon economy and sustainable development of the global community,[1,2] in recent years, researchers have wondered whether CO_2 could be utilized as an energy source.[3–5] Li–O_2/CO_2 batteries were first reported by Takechi *et al.*, who pointed out that the introduction of CO_2 into a battery system could increase the discharge capacity.[6] Attention was then drawn to a battery system that used CO_2 as a working gas, and the Li–CO_2 battery was born.[7–9] Capturing and converting CO_2 into an energy storage material not only reduces the accumulation of CO_2, but also reduces the use of fossil fuels. The rechargeable organic Li–CO_2 batteries reported so far, with the usual reaction mechanism: $4Li + 3CO_2 \rightleftarrows 2Li_2CO_3 + C$, have a theoretical energy density of 1876 W h kg^{-1}.[10–14] The many advantages of Li–CO_2 batteries have led researchers to develop a variety of materials to improve their performance, but research in this area is still in its early stages due to many insurmountable problems and challenges.[4,14,15] For example, the discharge product of Li–CO_2, Li_2CO_3, a wide bandgap insulator that is difficult to decompose, tends to create buildup in the battery, which in turn reduces the reversibility of the reaction and affects the cycle life.

It is important to develop high-performance catalysts to improve the charging and discharging process of Li–CO_2 batteries. Recently, covalent organic frameworks (COF) have shown great promise in the fields of gas storage, adsorption and catalysis due to their large specific surface area, tunable structure, easy functionalization and excellent chemical stability.[15,16] The design of COF materials has become an effective measure to provide pores and active sites for Li^+ transfer and CO_2 transport.[17–19] The COF material is utilized as a CO_2 collector during the discharge process to increase the discharge capacity, and also to promote the decomposition of Li_2CO_3 during the charging process. Li *et al.* reported an efficient COF cathode consisting of a hybrid of a hydrazone COF and Ru nanoparticles decorated with carbon nanotubes, which exhibited the ability to accelerate the decomposition of the discharge product Li_2CO_3.[20] Exfoliated nanosheets synergistically integrated with MnO_2 were designed by Jiang *et al.* as Li–CO_2 battery catalysts with ultra-high discharge capacity, demonstrating a new path for exploring porous crystalline materials as efficient cathode catalysts for Li–CO_2 batteries.[21] Among the numerous COF materials, the imine-based COFs are formed by the co-condensation of aldehydes and amines, with high physical and chemical stability and adjustable structural sites, which are favorable for their use in various fields.[22] By selecting suitable organic ligands to modify these, COF-based catalysts with high catalytic activity and excellent CO_2 adsorption capacity could be obtained.[23,24] Researchers have carried out many studies of the abundant transition metal Cu as the efficient catalyst due to its

Centre for Hydrogenergy, College of Materials Science and Technology, Nanjing University of Aeronautics and Astronautics, Nanjing 210016, P. R. China

† Electronic supplementary information (ESI) available. See DOI: https://doi.org/10.1039/d4sc07485h

advantages in CO_2 adsorption and storage.[25–28] Hu *et al.* synthesized BTA-COF–Cu with a Kagome lattice and Cu active sites, and the synergistic effect of the two promoted CO_2 adsorption/activation, facilitated photogenerated carrier migration, and induced the reduction of CO_2 to propene.[24] In summary, the functional groups of imine-based COF materials are able to coordinate with metals as active sites for catalysis, which enables COF to be used as a foundation for constructing high-level catalysts. Inspired by these, we designed to anchor the transition metal Cu as a catalytic site on the structural site of an imine-based COF to serve as an efficient cathode catalyst for Li–CO_2 batteries.

Here, we prepared Li–CO_2 battery catalysts with Cu–O,N active sites by utilizing the Schiff base reaction between the imine group and methoxy group and introducing Cu. At a current density of 200 mA g^{-1}, the prepared batteries were able to achieve effective reduction and oxidation of CO_2 with stable cycling for more than 110 cycles. This design of transition metals combined with COF sites provides a new method for realizing Li–CO_2 batteries for large-scale applications.

Experimental

Materials

1,3,5-Tris(4-aminophenyl)benzene (TAPB) and 2,5-dimethoxy benzene-1,4-dicarboxaldehyde (DMTP) were purchased from Bide Pharmatech Co., Ltd. 1,4-Dioxane, acetic acid, tetrahydrofuran (THF), and methanol were purchased from Shanghai Macklin Biochemical Technology Co., Ltd. *n*-Butanol and acetone were purchased from Nanjing Chemical Reagent Co., Ltd. All reagents were used as purchased commercially without any further purification.

Synthesis of Cu–TDCOF

The synthesis of TDCOF was based on the reported literature.[29] 6 mL of 1,4-dioxane, 6 mL of *n*-butanol and 1.5 mL of methanol solution were measured out, and 36.5 mg of TAPB and 26.1 mg of DMTP powder were weighed out. The above powders were mixed with the solution, and a freshly prepared 12 mol L^{-1} acetic acid solution was added as a catalyst to the homogeneous solution and allowed to stand for 30 minutes. The reaction kettle was kept at 70 °C for 24 h. TDCOF powder was washed with tetrahydrofuran at 8000 rpm three times and dried completely. 50 mg of ground TDCOF powder was weighed out and mixed with 15 mL of acetone in a glass vial. 34.1 mg of $CuCl_2 \cdot 2H_2O$ was weighed out and added to 10 mL of acetone, with ultrasonic mixing to achieve uniformity. The prepared $CuCl_2$ acetone solution was slowly added into a glass bottle under stirring, followed by magnetic stirring for 24 h at room temperature, washing and drying to obtain the Cu–TDCOF materials.

Electrochemical tests

Carbon paper was used as the current collector, and the mixed slurry (Cu–TDCOF : PVDF : Super P = 8 : 1 : 1) was loaded onto it; the mass loading of Cu–TDCOF and TDCOF was 0.2 mg. It was dried in a vacuum at 60 °C for 12 h. The dry electrode plate can be used as a cathode for Li–CO_2 batteries. Fresh lithium metal served as the anode, glass fiber as the membrane, and 1.0 M LiTFSI/DMSO as the electrolyte. The Li–CO_2 batteries were placed in sealed glass bottles filled with carbon dioxide gas and stabilized at 25 °C for 6 h before testing. Electrochemical impedance spectroscopy (EIS) was conducted using a Bio-Logic SP-200 (France). Cyclic voltammetry (CV) curves were measured using a CHI 600E. A LAND CT2001A battery test system was used to record the electrochemical performance of the batteries.

Material characterization

The X-ray diffraction (XRD) spectra were obtained using a Rigaku Ultimate IV, with Cu Kα radiation ($\lambda = 1.5406$ Å) and a speed of 5° min^{-1}. Scanning electron microscopy (SEM) was conducted using a Hitachi Co. S4800. High-resolution transmission electron microscopy (HR-TEM) and corresponding energy dispersive spectrometry (EDS) were performed using a JEOL JEM 2100F. The chemical composition was measured *via* inductively coupled plasma optical emission spectroscopy (ICP-OES) using a PerkinElmer Optima 8000 ICP-OES spectrometer. X-ray photoelectron spectroscopy (XPS) was carried out using a Thermo Scientific K-Alpha spectrometer. The Fourier transform infrared (KBr pellets) spectra were recorded in the range of 400–4000 cm^{-1} using a Thermo Nicolet 5700 FT-IR instrument. The special aberration corrected transmission electron microscopy (AC-TEM) was conducted using a JEOL ARM200F.

Results and discussion

In this paper, Cu was introduced into an imine-based COF to form the Cu–O,N active site to prepare the catalyst Cu–TDCOF; the synthesis route and battery schematic are shown in Fig. 1 and S1.† As shown in Fig. 2a–c, the morphological features of Cu–TDCOF were observed using SEM and TEM, and it was found that Cu–TDCOF exhibited a spherical nanoparticle shape consistent with that of TDCOF (Fig. S2†). The spherical particle structure endows the catalyst with an excellent interface for gas adsorption and electrochemical reactions for high active surface area in the Li–CO_2 batteries. From the TEM images, it was found that the surface of the nanorods was smooth and flat, and as shown in Fig. 2c, the surface of Cu–TDCOF showed very weak lattice streaks, confirming a certain crystallinity of the material. To observe the Cu sites clearly, we further performed AC-TEM tests and found that the bright spots of the Cu atoms were randomly dispersed on the COF carriers without forming clusters or nanoparticles (Fig. 2d). The results of EDS confirm the homogeneous distribution of the elements Cu, C, N and O in the structure of the spherical Cu–TDCOF particles (Fig. 2e). Moreover, according to the ICP-OES test results, the mass ratio of Cu is 7.02%.

The crystal structures of Cu–TDCOF and TDCOF powders were determined using XRD. The diffraction peaks located at 5.6°, 7.4°, and 9.7° in Fig. 3a correspond to the (200), (210), and (220) crystal planes of the composites, respectively, suggesting that the TDCOF exhibits a two-dimensional stacked structure,

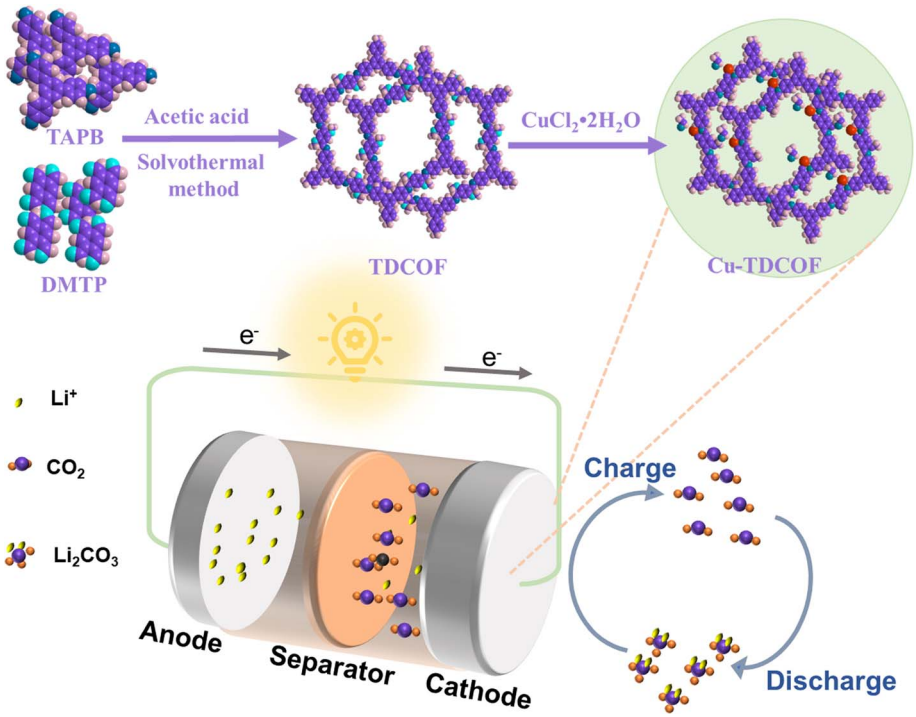

Fig. 1 Schematic synthesis of Cu–TDCOF and its use in a Li–CO_2 battery as a cathode catalyst.

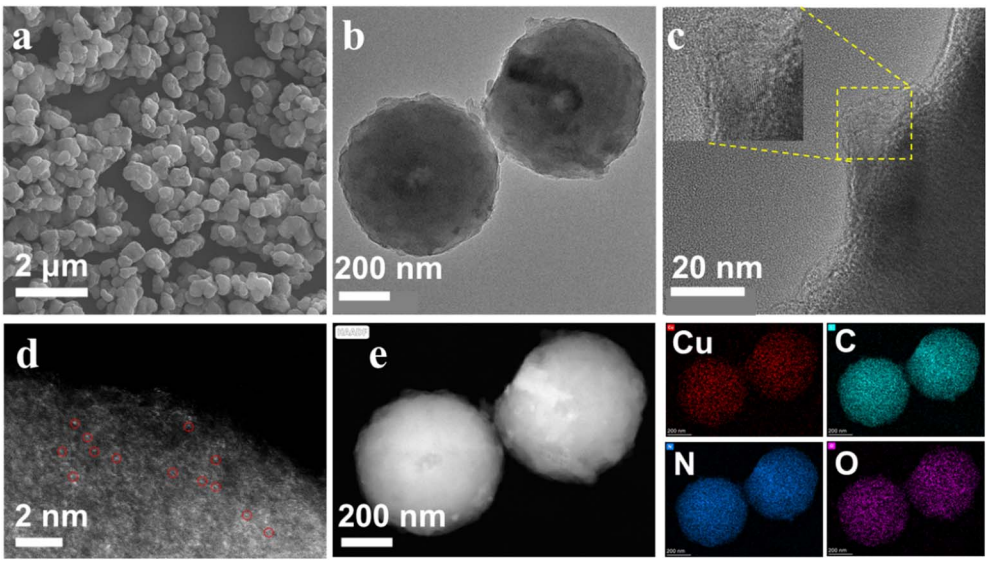

Fig. 2 (a) SEM images, (b) and (c) TEM images (inset image in (c) is an enlargement of the yellow dashed box with a size of 4 nm), (d) AC-TEM images, and (e) STEM images and element mappings of Cu, C, N, and O of the Cu–TDCOF sample.

which is in good agreement with previous studies.[29–32] The properties of Cu–TDCOF are consistent with those of TDCOF, with no obvious metallic phases, suggesting that the structure of TDCOF is preserved. The FT-IR of the Cu–TDCOF, TDCOF composites are shown in Fig. S3.† The C=N bond peaks of the Schiff base reaction are obvious, which confirms the successful preparation of the COF materials.[29] In order to identify the chemical state and coordination environment of Cu in the Cu–TDCOF material, it was analyzed using XPS (Fig. 3b–f). The C 1s spectrum can be fitted to the two diffraction peaks, C–O (285.78 eV) and C–C (284.8 eV), and the fitted peaks of C 1s of Cu–TDCOF and TDCOF are basically the same, which indicates that the introduction of Cu does not affect the structure of TDCOF, which is consistent with the XRD test results (Fig. 3c). As shown in Fig. 3d, compared with the main O 1s peak for TDCOF, the O 1s spectrum of Cu–TDCOF exhibits an additional peak corresponding to the formation of Cu–O bonds in Cu–TDCOF.[26] In the N 1s spectrum shown in Fig. 3e, in addition to the main

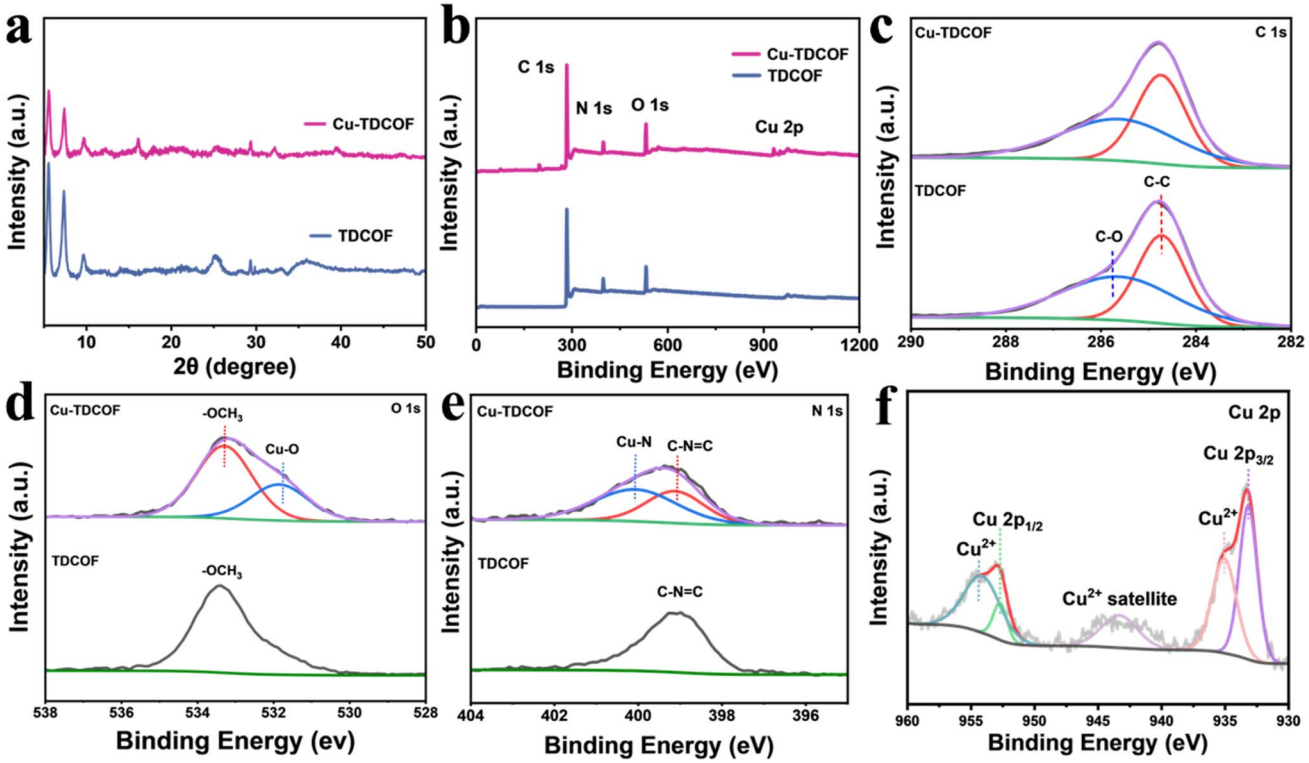

Fig. 3 Spectrogram characterization of Cu–TDCOF and TDCOF. (a) XRD spectra; (b) survey, (c) C 1s, (d) O 1s, (e) N 1s, and (f) Cu 2p XPS spectra.

peak of C–N=C, a shoulder peak with a higher binding energy of 400.08 eV was fitted, indicating the presence of Cu–N bonds.[26] In addition, the Cu 2p spectrum was fitted to Cu $2p_{3/2}$ and Cu $2p_{1/2}$ orbitals, with Cu mainly in the form of Cu^{2+} (Fig. 3f).[33] This suggests that the Cu atoms coordinate with the N and O atoms in the COF to form Cu–O,N sites on the COF surface, which act as catalytic sites for CO_2 reduction and oxidation.

In order to systematically compare the effects of Cu–O,N site construction on the electrochemical activity of Li–CO_2 batteries, the constant-current discharge curves and the depth of discharge of Cu–TDCOF and TDCOF at a current density of 200 mA g^{-1} were first compared. As shown in Fig. 4a, the discharge capacity of Cu–TDCOF is much higher than that of TDCOF and it has a higher discharge plateau. Notably, the battery with Cu–TDCOF as the cathode shows almost no capacity release under an Ar environment, as shown in Fig. S4.† The lower electrochemical impedance values of Cu–TDCOF similarly confirm the effect of the introduction of Cu on the electron transport velocity and improved electrochemical performance (Fig. 4b). In addition, the cyclic voltammetry (CV) curves of the Cu–TDCOF catalyst batteries were measured at a scan rate of 0.1 mV s^{-1} over the voltage range of 2.0 V to 4.5 V. The CV curves of the Cu–TDCOF catalyst batteries showed higher peak currents, suggesting that they have a higher capacity for CO_2 reduction and oxidation (Fig. S5†). No redox peaks appeared, with only oxidation of the electrolyte, in the Ar environment under the same conditions. The oxidation peak near 3.5 V corresponds to the oxidation of the electrolyte (Fig. S6†), which together, with the absence of capacity release of the battery under an Ar atmosphere confirmed CO_2 as an active substance in the system.

The rate capability of Li–CO_2 batteries with different cathodes was also investigated. The Cu–TDCOF cathode showed low discharge and charge voltage fluctuations as the current density was increased from 100 mA g^{-1} to 2000 mA g^{-1} (Fig. 4c and d). On the contrary, as the current density increased from 100 mA g^{-1} to 2000 mA g^{-1}, the TDCOF cathode showed significant polarization, and the battery polarization voltage increased from 1.3 V to 2.2 V. A comparison of the corresponding overpotentials of the different cathodes at different current densities is shown in Fig. 4d. The potential difference of the Cu–TDCOF cathode always remains below 1.8 V, and when the current density was reverted to 100 mA g^{-1}, the Cu–TDCOF battery was restored almost to the initial voltage plateau, which demonstrated its remarkable stability, suggesting that the Cu–O,N active sites played an active role.[26] To assess its cycling stability and practicality, Cu–TDCOF cycling performance was tested. The overpotential of the Cu–TDCOF cathode increased by only 0.8 V at a current density of 200 mA g^{-1} and a rated capacity of 1000 mA h g^{-1} after a long cycling period of over 1100 h (Fig. 4g). Using the TDCOF cathode under the same test conditions, the discharge voltage plummeted after 600 h of cycling (Fig. S7†). This phenomenon can be attributed to round-trip redox reactions during cycling, suggesting that it is challenging to maintain long-term cycling stability using pure COF materials alone. During the cycling process of the battery, the insulating discharge product Li_2CO_3 continuously accumulates

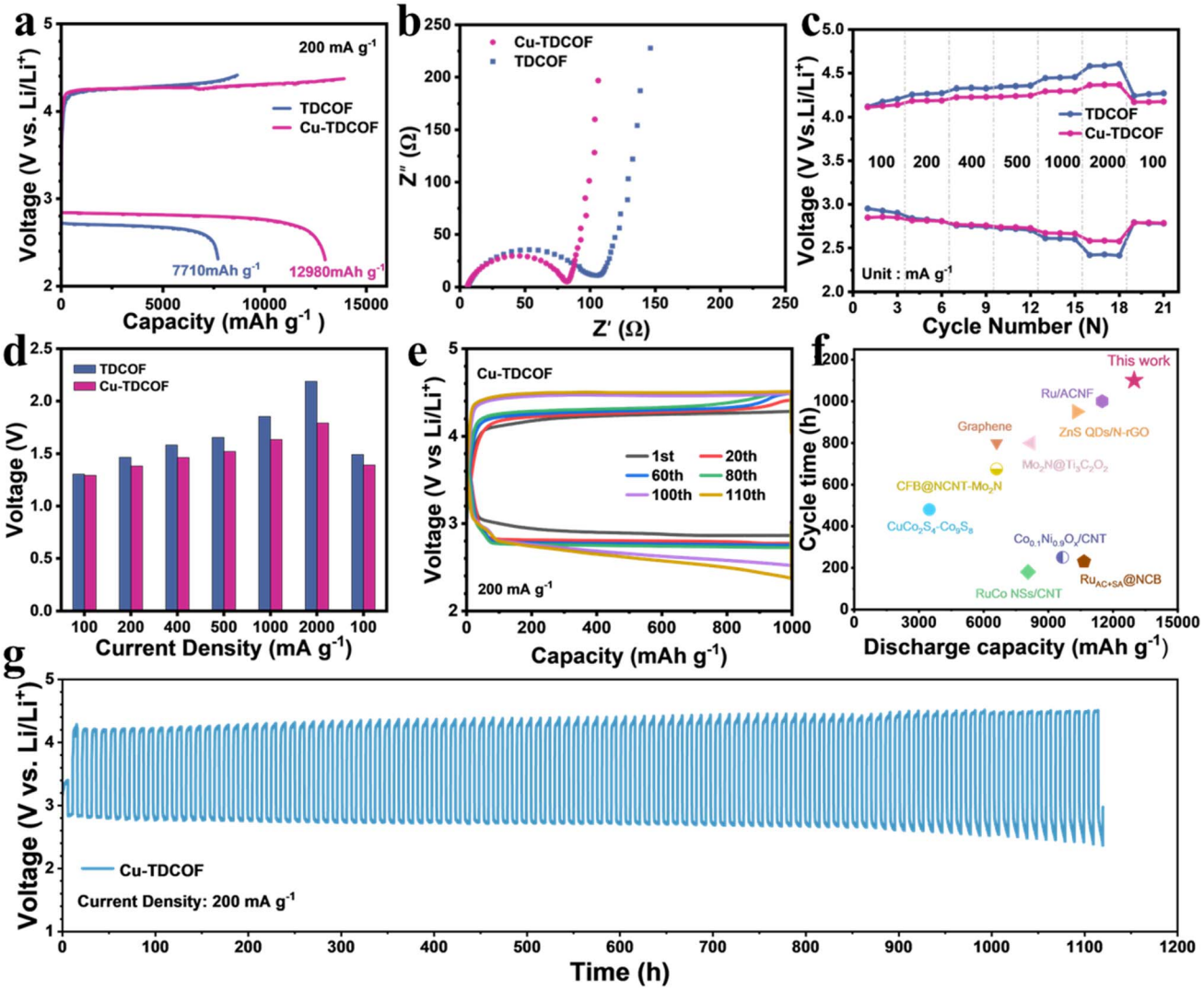

Fig. 4 Electrochemical performances of Cu–TDCOF for Li–CO_2 batteries. (a) Full discharge and charge capacities of Cu–TDCOF and TDCOF at 200 mA g^{-1}. (b) EIS spectra of Cu–TDCOF and TDCOF for Li–CO_2 batteries. (c) Rate performances at a different current densities (100, 200, 400, 500, 1000, and 2000 mA g^{-1}). (d) Overpotential of the Cu–TDCOF and TDCOF Li–CO_2 battery at different current densities. (e) Cycle performances of Cu–TDCOF at a limited capacity of 1000 mA h g^{-1} at 200 mA g^{-1}. (f) Comparison between Cu–TDCOF and reported excellent Li–CO_2 batteries catalysts, focusing on discharge capacity and cycle time. (g) Voltage/time curves of Cu–TDCOF at 200 mA g^{-1} with a limited capacity of 1000 mA h g^{-1}.

at the cathode to cover the active sites and requires higher energy input to decompose, which leads to the increasing overpotential of the battery and the gradual decrease in the cycling stability until deactivation.[34] In addition, we tested the cycling performance at 500 mA g^{-1} under limited capacities of 8000 and 1000 mA h g^{-1}. As shown in Fig. S8,† under smaller capacity, the battery can maintain a stable charge/discharge voltage for than 120 h without significant degradation. The extra-large capacity battery no longer maintains a stable discharge voltage after only one cycle, and the battery is unable to maintain long-lasting cycling at a larger capacity. Therefore, determining how to realize the full discharge–charge of Li–CO_2 batteries is one of the directions for future research. Fig. 4f illustrates a comparative analysis between Cu–TDCOF and the state-of-the-art catalysts reported in the literature, focusing on cycle time and discharge capacity (detailed information is presented in Table S1†).[35–43] The excellent stability of TDCOF and the high catalytic activity of the Cu–O,N sites in the CO_2 redox process endowed Cu–TDCOF with excellent charging and discharging performance.[26,44]

The formation and decomposition of discharge products and the corresponding electrochemical reaction mechanism are the core of the operation of Li–CO_2 batteries.[45–47] The electrochemical process of Li–CO_2 batteries involves charge transfer processes at the multiphase interfaces, which include the solid state (catalysts, discharge products), the gaseous state (CO_2 gas), and the liquid state (electrolyte), and the different products correspond to different electrochemical processes with different performances.[15,48] In order to study the working principle of Cu–TDCOF in Li–CO_2 batteries, we investigated the

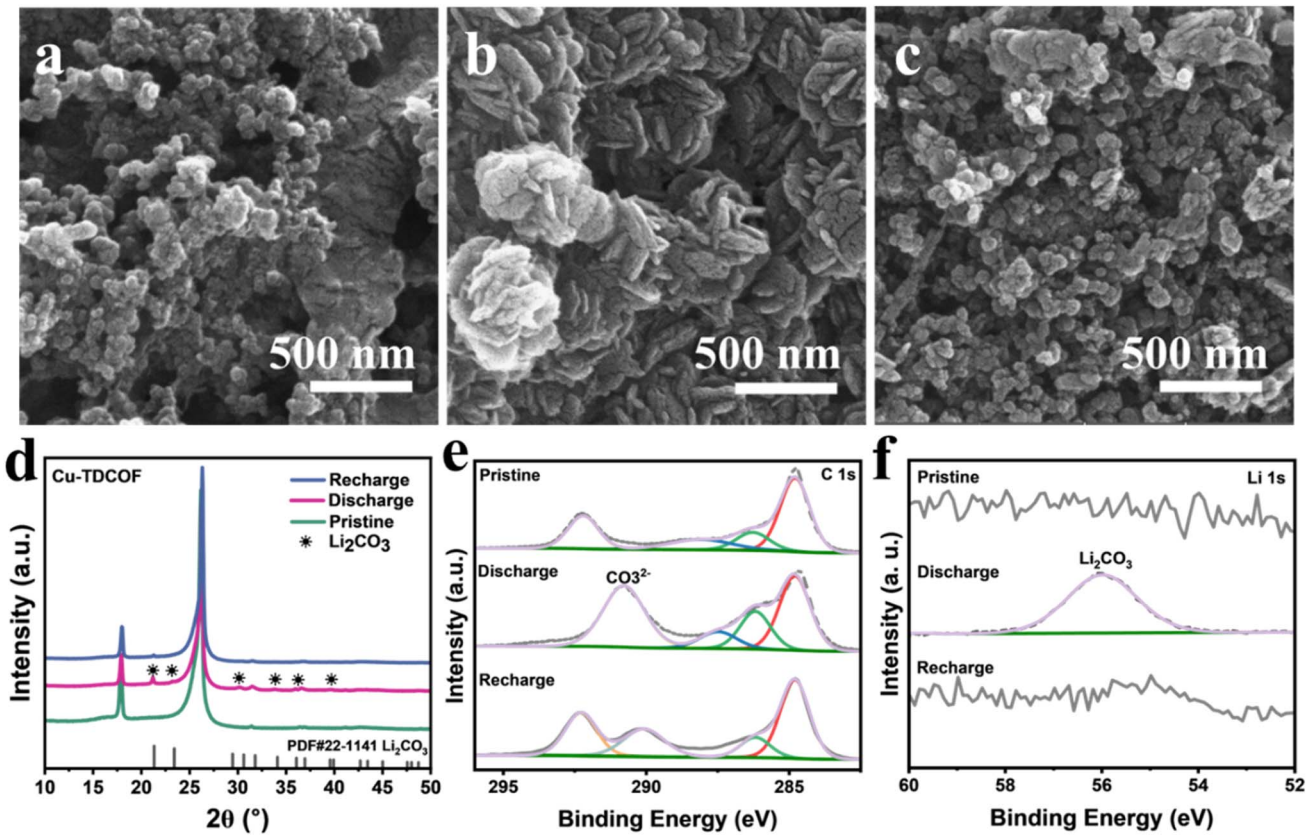

Fig. 5 (a–c) SEM images of Cu–TDCOF in the pristine, discharged, and recharged states. (d) XRD and (e and f) XPS spectra of Cu–TDCOF in the pristine, discharged, and recharged states.

cathode changes in different states *via* SEM, XRD and XPS analysis. The results showed that a large number of flaky discharge products uniformly accumulated to form a "rose"-like shape; they are distributed on the electrode surface and completely disappear after recharging (Fig. 5a–c and S9†). The XRD spectra (Fig. 5d) showed diffraction peaks corresponding to the Li_2CO_3 standard card (PDF#22-1141), confirming that the system undergoes a recyclable process based on the generation and decomposition of Li_2CO_3. In addition, the C 1s XPS spectra show diffraction peaks corresponding to carbonate (290.78 eV) at different positions during discharge compared to the initial electrode (Fig. 5e).[49] Combined with the Li 1s XPS results, it was concluded that the battery generated Li_2CO_3 during the discharge process (Fig. 5f), which was fully decomposed after charging.[50]

Conclusion

In summary, we have constructed a novel Li–CO_2 battery catalyst with Cu–O,N active sites by anchoring metal Cu to the structural sites of imine-based COF materials *via* a solvothermal method. Cu–TDCOF, which acts as a highly efficient electrocatalyst, is capable of accelerating the redox kinetics. The Li–CO_2 batteries based on Cu–TDCOF can maintain stable cycling for more than 1100 h at a current density of 200 mA g^{-1}. The Cu–O,N sites facilitate the accelerated electron transfer of the COF and serve as highly selective CO_2 reduction catalyst, assisting in the full decomposition of the discharge products. This work demonstrates the potential of modified COF materials as catalysts for CO_2 redox and Li-air batteries.

Data availability

The data supporting this study are available within the main text and the ESI.†

Author contributions

H. C., T. W., Y. T. and Y. X. designed the experiment and wrote the manuscript. H. C., Z. L., X. Y. and Y. L. conducted the experiments. X. H. and J. H. analyzed the data. All authors discussed the results at all stages and participated in the development of the manuscript.

Conflicts of interest

There are no conflicts of interest to declare.

Acknowledgements

The authors acknowledge the financial support for this work from the Fund Project for the National Defense Technology

Innovation Special Zone Spark Project (2016300TS00911901) and a Project Funded by the Priority Academic Program Development of Jiangsu Higher Education Institutions (PAPD). Postgraduate Research & Practice Innovation Program of NUAA (xcxjh20230608, and xcxjh20230614). This project is also supported by Jiangsu Provincial College Student Innovation Training Program Support Project (202410287169Y).

References

1 K. Peramaiah, M. Yi, I. Dutta, S. Chatterjee, H. Zhang, Z. Lai and K. Huang, *Adv. Mater.*, 2024, **36**, 2470410.
2 L. Wang, Y. Han, J. Wei, Q. Ge, S. Lu, Y. Mao and J. Sun, *Appl. Catal., B*, 2023, **328**, 122506.
3 W. Li and J. Luo, *Electrochem. Energy Rev.*, 2021, **4**, 518–544.
4 X. Mu, H. Pan, P. He and H. Zhou, *Adv. Mater.*, 2020, **32**, 1903790.
5 W. Ma, X. Liu, C. Li, H. Yin, W. Xi, R. Liu, G. He, X. Zhao, J. Luo and Y. Ding, *Adv. Mater.*, 2018, **30**, 1801152.
6 K. Takechi, T. Shiga and T. Asaoka, *Chem. Commun.*, 2011, **47**, 3463.
7 Z. Li, M. Li, X. Wang, D. Guan, W. Liu and J. Xu, *J. Mater. Chem. A*, 2020, **8**, 14799–14806.
8 X. Hu, Z. Li and J. Chen, *Angew. Chem., Int. Ed.*, 2017, **56**, 5785–5789.
9 J. Li, L. Wang, Y. Zhao, S. Li, X. Fu, B. Wang and H. Peng, *Adv. Funct. Mater.*, 2020, **30**, 2001619.
10 Y. Qiao, J. Yi, S. Wu, Y. Liu, S. Yang, P. He and H. Zhou, *Joule*, 2017, **1**, 359–370.
11 Q. Pan, X. Ma, H. Wang, Y. Shu, H. Liu, L. Yang, W. Li, J. Liu, Y. Wu, Y. Mao, J. Xie, G. Zou, H. Hou, W. Deng and X. Ji, *Adv. Mater.*, 2024, **36**, 2406905.
12 B. Chen, D. Wang, J. Tan, Y. Liu, M. Jiao, B. Liu, N. Zhao, X. Zou, G. Zhou and H. Cheng, *J. Am. Chem. Soc.*, 2022, **144**, 3106–3116.
13 S. Wang, K. Xu, H. Song, T. Zhu, Z. Yu, X. Song, D. Li, L. Yu, J. Xu and K. Chen, *Adv. Energy Mater.*, 2022, **12**, 2201866.
14 T. Jian, W. Ma, C. Xu, H. Liu and J. Wang, *eScience*, 2023, **3**, 100114.
15 H. Chen, X. Li, H. Xue, L. Jia, Y. Xu, Y. Tao, Y. Yan, X. Fan, J. He and T. Wang, *Inorg. Chem. Front.*, 2024, **11**, 5833–5857.
16 A. P. Côté, A. I. Benin, N. W. Ockwig, M. O'Keeffe, A. J. Matzger and O. M. Yaghi, *Science*, 2005, **310**, 1166–1170.
17 N. Yang, W. Yan, Z. Zhou, C. Tian, P. Zhang, H. Liu, X. Wu, C. Xia, S. Dai and X. Zhu, *Nano Lett.*, 2024, **24**, 5444–5452.
18 J. Hou, H. Liu, M. Gao, Q. Pan and Y. Zhao, *Angew. Chem., Int. Ed.*, 2024, **64**, e202414566.
19 X. Yang, X. Lan, Y. Zhang, H. Li and G. Bai, *Appl. Catal., B*, 2023, **325**, 122393.
20 X. Li, H. Wang, Z. Chen, H. Xu, W. Yu, C. Liu, X. Wang, K. Zhang, K. Xie and K. P. Loh, *Adv. Mater.*, 2019, **31**, 1905879.
21 C. Jiang, Y. Zhang, M. Zhang, N. Ma, G. Gao, J. Wang, M. Zhang, Y. Chen, S. Li and Y. Lan, *Cell Rep. Phys. Sci.*, 2021, **2**, 100392.
22 Z. Li, Y. Li, H. Cheng, Y. Song, Y. Jiao, S. Shi, J. Gao, L. Sun and J. Hou, *Appl. Catal., B*, 2024, **345**, 123698.
23 S. Huang, D. Chen, C. Meng, S. Wang, S. Ren, D. Han, M. Xiao, L. Sun and Y. Meng, *Small*, 2019, **15**, 1904830.
24 Y. Hu, G. Liu, T. Song, X. Hu, B. Long and G. Deng, *Appl. Catal., B*, 2025, **361**, 124587.
25 Y. Liu, S. Zhao, D. Wang, B. Chen, Z. Zhang, J. Sheng, X. Zhong, X. Zou, S. Jiang, G. Zhou and H. Cheng, *ACS Nano*, 2022, **16**, 1523–1532.
26 W. Tu, Y. Yang, C. Chen, T. Zhou, T. Li, H. Wang, S. Wu, Y. Zhou, D. O'Hare, Z. Zou and R. Xu, *Small Struct.*, 2023, **4**, 2200233.
27 L. Liu, S. Shen, N. Zhao, H. Zhao, K. Wang, X. Cui, B. Wen, J. Wang, C. Xiao, X. Hu, Y. Su and S. Ding, *Adv. Mater.*, 2024, **36**, 2403229.
28 X. Li, C. Li, X. Zhang, J. Sun, X. Liu, K. Song, J. Han, J. Wang and J. Chen, *Angew. Chem., Int. Ed.*, 2024, **63**, e202412533.
29 H. Xu, J. Gao and D. Jiang, *Nat. Chem.*, 2015, **7**, 905–912.
30 X. Sun, N. Wang, Y. Xie, H. Chu, Y. Wang and Y. Wang, *Talanta*, 2021, **225**, 122072.
31 Q. Cao, S. Zhang, L. Zhang, F. Gao, J. Chen, Y. Dong and X. Li, *ACS Appl. Mater. Interfaces*, 2021, **13**, 13693–13704.
32 T. Zhang, C. Gao, W. Huang, Y. Chen, Y. Wang and J. Wang, *Talanta*, 2018, **188**, 578–583.
33 W. Weng and J. Guo, *Nat. Commun.*, 2022, **13**, 5768.
34 X. Li, J. Zhou, J. Zhang, M. Li, X. Bi, T. Liu, T. He, J. Cheng, F. Zhang, Y. Li, X. Mu, J. Lu and B. Wang, *Adv. Mater.*, 2019, **31**, 1903852.
35 Z. Zhang, Q. Zhang, Y. Chen, J. Bao, X. Zhou, Z. Xie, J. Wei and Z. Zhou, *Angew. Chem., Int. Ed.*, 2015, **54**, 6550–6553.
36 Y. Qiao, S. Xu, Y. Liu, J. Dai, H. Xie, Y. Yao, X. Mu, C. Chen, D. J. Kline, E. M. Hitz, B. Liu, J. Song, P. He, M. R. Zachariah and L. Hu, *Energy Environ. Sci.*, 2019, **12**, 1100–1107.
37 H. Wang, K. Xie, Y. You, Q. Hou, K. Zhang, N. Li, W. Yu, K. P. Loh, C. Shen and B. Wei, *Adv. Energy Mater.*, 2019, **9**, 1901806.
38 L. Chen, J. Zhou, Y. Wang, Y. Xiong, J. Zhang, G. Qi, J. Cheng and B. Wang, *Adv. Energy Mater.*, 2023, **13**, 2202933.
39 R. Zheng, M. Yang, X. Zhu, Q. Fang, X. Wang, P. Lei, J. Zhou, B. Wang and J. Cheng, *Adv. Funct. Mater.*, 2024, **35**, 2412999.
40 X. Zhu, L. Chen, Q. Fang, J. Cheng, Y. Su, P. Ratajczak, F. Beguin and B. Wang, *ACS Sustain. Chem. Eng.*, 2024, **12**, 12755–12762.
41 X. Xiao, Z. Zhang, W. Yu, W. Shang, Y. Ma, X. Zhu and P. Tan, *ACS Appl. Energy Mater.*, 2021, **4**, 11858–11866.
42 Y. Wang, J. Zhou, C. Lin, B. Chen, Z. Guan, A. M. Ebrahim, G. Qian, C. Ye, L. Chen, Y. Ge, Q. Yun, X. Wang, X. Zhou, G. Wang, K. Li, P. Lu, Y. Ma, Y. Xiong, T. Wang, L. Zheng, S. Chu, Y. Chen, B. Wang, C. Lee, Y. Liu, Q. Zhang and Z. Fan, *Adv. Funct. Mater.*, 2022, **32**, 2202737.
43 J. Lin, J. Ding, H. Wang, X. Yang, X. Zheng, Z. Huang, W. Song, J. Ding, X. Han and W. Hu, *Adv. Mater.*, 2022, **34**, 2200559.
44 Y. Xu, X. Li, Y. Li, Y. Wang, L. Song, J. Ding, X. Fan, J. He, T. Wang and Z. Wu, *Energy Storage Mater.*, 2024, **68**, 103354.
45 C. Yang, K. Guo, D. Yuan, J. Cheng and B. Wang, *J. Am. Chem. Soc.*, 2020, **142**, 6983–6990.
46 H. Xue, H. Gong, X. Lu, B. Gao, T. Wang, J. He, Y. Yamauchi, T. Sasaki and R. Ma, *Adv. Energy Mater.*, 2021, **11**, 2101630.
47 J. Xie, Q. Liu, Y. Huang, M. Wu and Y. Wang, *J. Mater. Chem. A*, 2018, **6**, 13952–13958.

48 Z. Wang, L. Deng, X. Yang, J. Lin, D. Cao, J. Liu, Z. Tong, J. Zhang, G. Bai, Y. Luo, Z. Yin, Y. Zhou and J. Li, *Adv. Funct. Mater.*, 2024, **34**, 2404137.
49 K. P. C. Yao, D. G. Kwabi, R. A. Quinlan, A. N. Mansour, A. Grimaud, Y. Lee, Y. Lu and Y. Shao-Horn, *J. Electrochem. Soc.*, 2013, **160**, A824–A831.
50 M. Asadi, B. Sayahpour, P. Abbasi, A. T. Ngo, K. Karis, J. R. Jokisaari, C. Liu, B. Narayanan, M. Gerard, P. Yasaei, X. Hu, A. Mukherjee, K. C. Lau, R. S. Assary, F. Khalili-Araghi, R. F. Klie, L. A. Curtiss and A. Salehi-Khojin, *Nature*, 2018, **555**, 502–506.